3676–3689 *Nucleic Acids Research, 2008, Vol. 36, No. 11* *Published online 13 May 2008*
doi:10.1093/nar/gkn170

Streptococcus pyogenes pSM19035 requires dynamic assembly of ATP-bound ParA and ParB on *parS* DNA during plasmid segregation

Florencia Pratto[1], Aslan Cicek[2], Wilhelm A. Weihofen[2], Rudi Lurz[3], Wolfram Saenger[2] and Juan C. Alonso[1,*]

[1]Department of Microbial Biotechnology, National Centre of Biotechnology, CSIC, 28049 Madrid, Spain, [2]Institute of Chemistry and Biochemistry / Crystallography, Freie Universität Berlin, 14195 and [3]Max-Planck Institute for Molecular Genetics, 14195 Berlin, Germany

Received January 8, 2008; Revised March 19, 2008; Accepted March 25, 2008

ABSTRACT

The accurate partitioning of Firmicute plasmid pSM19035 at cell division depends on ATP binding and hydrolysis by homodimeric ATPase δ_2 (ParA) and binding of ω_2 (ParB) to its cognate *parS* DNA. The 1.83 Å resolution crystal structure of δ_2 in a complex with non-hydrolyzable ATPγS reveals a unique ParA dimer assembly that permits nucleotide exchange without requiring dissociation into monomers. *In vitro*, δ_2 had minimal ATPase activity in the absence of ω_2 and *parS* DNA. However, stoichiometric amounts of ω_2 and *parS* DNA stimulated the δ_2 ATPase activity and mediated plasmid pairing, whereas at high (4:1) ω_2:δ_2 ratios, stimulation of the ATPase activity was reduced and δ_2 polymerized onto DNA. Stimulation of the δ_2 ATPase activity and its polymerization on DNA required ability of ω_2 to bind *parS* DNA and its N-terminus. *In vivo* experiments showed that δ_2 alone associated with the nucleoid, and in the presence of ω_2 and *parS* DNA, δ_2 oscillated between the nucleoid and the cell poles and formed spiral-like structures. Our studies indicate that the molar ω_2:δ_2 ratio regulates the polymerization properties of $(\delta\bullet ATP\bullet Mg^{2+})_2$ on and depolymerization from *parS* DNA, thereby controlling the temporal and spatial segregation of pSM19035 before cell division.

INTRODUCTION

Accurate distribution of newly replicated chromosomes before cell division is imperative for the stable transmission of genetic information. In eukaryotic cells, after chromosomal DNA condensation and alignment at mid-cell, microtubule fibers anchored via the kinetochore to the centromere pull the sister chromatids apart (1,2). In bacterial cells the mechanism that moves the newly replicated chromosomes and plasmids to opposite sides of the division plane requires a genuine partition system (ParA and ParB, ParM and ParR, or TubZ and TubR) (2–6).

For active and faithful segregation, most bacterial chromosomes and low-copy-number plasmids have evolved genuine partitioning (*par*) loci. The *par* loci contain one or more *cis*-acting DNA segment(s) (*parS*) and encode two *trans*-acting proteins: an ATPase motor protein and a centromere binding protein (3–5,7,8). Three evolutionary different plasmid partition systems have been identified: the tubulin-like (TubZ or type III), the actin-like (ParM or type II), and the Walker-box (ParA or type I) ATPases (4–6,9,10). The ParA system, which is the most common and conserved one, can be subdivided into two subfamilies (ParA-Ia and ParA-Ib) (4). The mechanism of action of ParA systems is less clear than that of the other mentioned systems, although a similar mechanism to the one observed with the actin-like systems has been suggested (3–5,7,8). Among the Proteobacteria phylum a large number of plasmid- and chromosome-encoded partition systems have been studied, e.g. plasmids P1, F and RK2 encode ParA-Ia ATPases (P1-ParA, F-SopA and RK2-IncC), while plasmids pB171 and pTB228 and the *Caulobacter crescentus* (*Ccr*) chromosome encode ParA-Ib ATPases (pB171-ParA, pTB228-ParF and *Ccr*ParA). However, among the Firmicutes phylum the ParA ATPases studied thus far (e.g. *Streptococcus pyogenes* pSM19035 and the *Bacillus subtilis* chromosome) encode ATPase of the ParA-Ib (δ_2 and *Bsu*Soj) subfamily [(3–5), this work]. The ParA-Ia

*To whom correspondence should be addressed. Tel: +34 91585 4546; Fax: +34 91585 4506; Email: jcalonso@cnb.csic.es
Present address:
Wilhelm A. Weihofen, Department of Molecular and Cellular Biology, Harvard University, MA 02138, USA
The authors wish it to be known that, in their opinion, the first two authors should be regarded as joint First Authors

ATPases feature an N-terminal helix-turn-helix (HTH) motif that specifically interacts with DNA to repress the expression of the *par* loci, while the ParA-Ib ATPases bind non-specifically to DNA [e.g. δ_2 and *Thermus thermophilus* Soj (*Tth*Soj)] (3–5).

The ParB proteins are divided into three discrete subfamilies (ParB-I, -II and -III) (3–5). The ParB-I proteins (e.g. P1-ParB, F-SopB or RK2-KorB), and ParB-II proteins (e.g. *Bsu*Spo0J or *Tth*Spo0J) recognize *parS* DNA via an HTH fold and '*spread*' around the *parS* site. The ParB-III proteins (e.g. pB171-ParB, pTB228-ParG, pSM19035-ω_2) work in concert with ParA-Ib ATPases and recognize *parS* (*parC*) DNA via a ribbon-helix-helix (RHH) motif. The *cis*-acting *parS* DNA consists of one (e.g. P1-*parS*, F-*sopC*), two (e.g. pB171-*parC*) or several copies of the centromeric *parS* site (e.g. pSM19035-*parS, Bsu-parS*) (3–5,8).

Plasmid partitioning has mainly been studied in species of the γ Proteobacteria phylum (3–5,8). The polymerization of $(\delta\bullet ATP\bullet Mg^{2+})_2$ on DNA (see below), which is in stark contrast to ParA ATPases of γ proteobacterial plasmids that form proteofilaments in the absence of ParB and DNA, suggests that the dynamic movement of plasmid and bacterial chromosomes during faithful segregation in Firmicutes may not necessarily follow similar mechanisms as found for plasmids of γ Proteobacteria [(5), this work]. Indeed, the evolutionary distance between *B. subtilis* or *Streptococcus pyogenes* (Firmicutes) and *E. coli* (γ Proteobacteria) exceeds that between plants and animals, and this raises the question whether bacteria of these two phyla share the same mechanism of plasmid partitioning. Here, we address this question by studying the segregation of plasmid pSM19035 originally isolated from the Firmicute and human pathogen *S. pyogenes*.

Plasmid pSM19035 replicates via a theta mechanism and is maintained stably at 1–3 copies per cell in *B. subtilis*, as well as in a wide range of species of the Firmicutes phylum (11–13). The *par* locus of pSM19035 encodes two *trans*-acting proteins, δ (ParA-Ib type) and ω (ParB-III type) and harbors six *cis*-acting *parS* sites [(14–16), this work]. Protein δ, which occurs as a homodimer (δ_2), shares sequence identity with bacterial and archaeal Walker-box ATPases, namely *Tth*Soj and *Pyrococcus furiosus* MinD (*Pfu*MinD) [(11), Figure S1 in the Supplementary Data available with this article online]. Protein ω, which occurs as a homodimer (ω_2), acts as a multifunctional repressor of genes involved in copy number control, plasmid addiction and accurate segregation [(15), this work]. Repressor ω_2 negatively controls promoter utilization by binding cooperatively and with high affinity to the promoter regions upstream of *copS*, δ and ω genes (P_{copS}, P_δ and P_ω). These regions, which function as the *cis*-acting *parS* sites (*parS*1 or P_δ, *parS*2 or P_ω and *parS*3 or P_{copS}, Figure 1A and B), contain 10, 7 and 9 unspaced heptads with sequence 5′-WATCACW-3′ in (→ or ←) orientations (15). The affinities of ω_2 for the cognate sites P_{copS}, P_ω and P_δ are similar with a k_D of ~6 nM [(17), Figure 1B]. The minimal cooperative yet high affinity binding sites for ω_2 are two contiguous heptads in direct (→→) or inverted (→←) orientations (*minimal centromere*) (17).

The N-terminal region of protein ω_2 is unstructured (18,19). Crystal structures have been determined for protein ω_2 in which the monomers lack the first 20 N-terminal amino acid residues ($\omega_2\Delta$N20) (20) and for $\omega_2\Delta$N19 in complex with two diheptads in (→→) and (→←) orientations (21). Chemical and enzymatic footprint data of ω_2 binding to the centromere reveal a continuous protein super-structure consistent with the crystal structures (21). Extrapolating from these structures, $\omega_2\Delta$N19 molecules assemble as a left-handed protein helix that wraps *parS* sites consisting of multiple DNA heptad repeats (Figure 1C). The abilities of $\omega_2\Delta$N19 and wild-type (wt) ω_2 to bind to *parS* DNA *in vitro* and to repress transcription *in vivo* are comparable, but substitution of Threonine 29 (that binds specifically to the central G–C base pair of the heptads) for Alanine (ω_2T29A) abolishes DNA binding (18,19,21).

Here, we provide the first crystal structure of a plasmid-encoded ParA-Ib type protein in the ATPγS-bound state $(\delta\bullet ATP\gamma S\bullet Mg^{2+})_2$ and show that plasmid pairing, polymerization of $(\delta\bullet ATP\bullet Mg^{2+})_2$ on and depolymerization from *parS* DNA, which is dependent on wt ω_2 bound to *parS* DNA, is fine tuned by the stoichiometry of ω_2 and δ_2. This is consistent with the dynamic assembly of a partition apparatus through the interaction of $(\delta\bullet ATP\bullet Mg^{2+})_2$ with $\omega_2\bullet$*parS* complexes and supports a model proposed here for DNA segregation in Firmicutes that is mediated by δ_2 (ParA) plus ω_2 (ParB) and differs from that in γ proteobacteria plasmids.

MATERIALS AND METHODS

Plasmid stability test

The bacterial strains and plasmids used are listed in Supplementary Table S1. The numbers of plasmid-containing cells were determined by replica plating onto chloramphenicol-containing plates. The theoretical frequency of plasmid loss ($L_{th} = 2^{1-n}$) is the probability of plasmid-free cells arising per division, with n being the number of copies of the plasmid per cell at cell division (12). The frequency of plasmid loss (L) was calculated as $L = 1 - (P)^{1/g}$, where P is the number of cells bearing plasmids after growth for g generations.

Protein expression and purification

Proteins ω, ωΔN19 or ωT29A were expressed in *E. coli* BL21(DE3) pLysS cells and purified as described (17,18). Proteins δ, δK36A, δD60A or δ_{+14} (having 14 extra N-terminal residues when compared to δ) were expressed in *E. coli* ER2566 cells and purified by sequential heparin POROS 20HE (buffer A, 50 mM Tris–HCl, pH 8.0, 2 mM EDTA) containing 0.05 to 1 M NaCl concentrations, anion-exchange PL-SAX (buffer A containing increasing NaCl concentrations) and gel-filtration chromatography (buffer B, 20 mM Tris–HCl, pH 8.0, 200 mM NaCl). The protein concentrations were determined by absorption at 280 nm using molar extinction coefficients of $2980\,M^{-1}\,cm^{-1}$ for ω_2, $\omega_2\Delta$N19 and ω_2T29A, and $38\,850\,M^{-1}\,cm^{-1}$ for δ_2, δ_2K36A and δ_2D60A, and concentrations are specified for protein dimers.

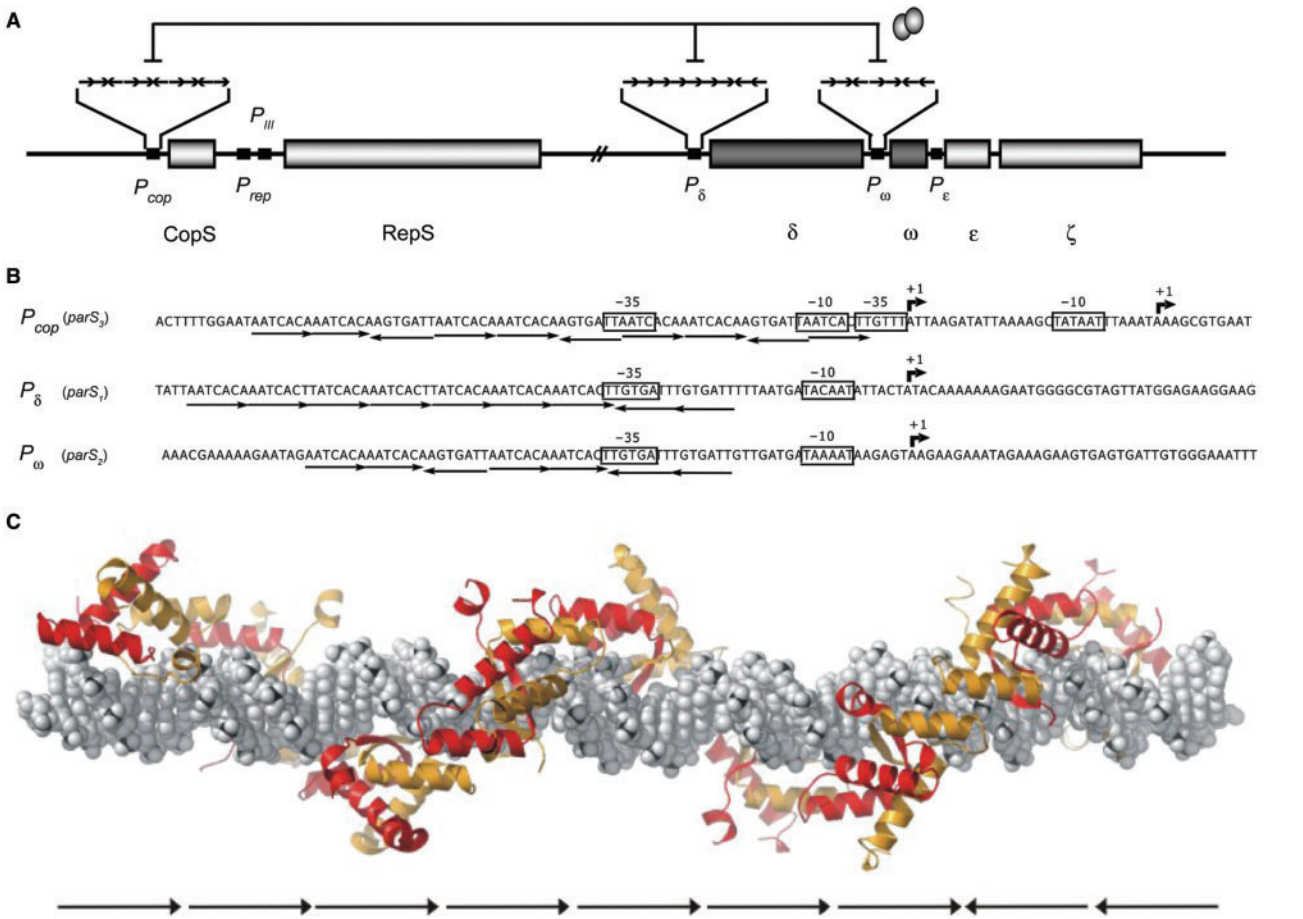

Figure 1. Genome organization, nucleotide sequences of the ω_2-binding sites and proposed structure of the ω_2•*parS*1 (P_{δ}) complex. (**A**) Organization of the genes that direct replication (*repS*) and its control (*copS*), segregation (δ, ω) and post-segregation growth inhibition (ε, ζ). This DNA segment is duplicated in pSM19035 (14,15). The promoter (*P*) regions (P_{cop}, P_{III}, P_{rep}, P_{δ}, P_{ω} and P_{ε},) of one arm of the plasmid, and the directions of the ω_2 binding sites (7-bp heptad repeats 5′-WATCACW-3′, W is A or T, symbolized by → or ←) are identified by arrows. Repression of P_{cop}, P_{δ} and P_{ω} by ω_2 is indicated by the two ellipsoids. (**B**) Sequences of the P_{cop} (*parS*3), P_{δ} (*parS*1) and P_{ω} (*parS*2) regions with −35 and −10 regions are boxed and transcription start sites indicated by bent arrows. The heptads are indicated by arrows. (**C**) Model of nine ω_2 bound to *parS* DNA based on the crystal structures determined for $[\omega_2\Delta N19]_2$-(→→) and $[\omega_2\Delta N19]_2$-(→←) complexes (21) with the DNA shown in space filling (gray/blue) and ω_2 in ribbon representations (one monomer is orange, the other red).

Co-crystallization, data collection and structure determination

Crystals in space group $P6_522$ grew at 18°C in sitting drop vapour diffusion setups from 1 µl protein solution (14 mg δ_2/ml, buffer B with 2 mM ATPγS and 5 mM $MgCl_2$) mixed with 1 µl of buffer C (1 M Hepes and 3% (v/v) ethanol pH 7.0). The mother liquor was supplemented with glycerol to a final concentration of 25% (v/v) prior to flash freezing the crystals in liquid N_2.

X-ray diffraction data were collected at 100 K at Protein Structure Factory beamline BL1 of Freie Universität Berlin at BESSY and processed with DENZO/Scalepack (22). The structure was determined by molecular replacement using a monomer of the *Tth*Soj protein structure (pdb code 2BEJ) as a search model. The model of δ was built and water molecules were located with ARP/wARP (23). Restrained refinement cycles in REFMAC5 (24) converged at an *R* factor (R_{free}) of 19.2% (21.8%) (Table 1). Atomic coordinates and structure factors have been deposited with the Protein Data Bank under accession code 2OZE.

ATPase activity assay

ATPase activity was assayed by thin-layer chromatographic separation of the reaction products. Reaction mixtures (20 µl) contained buffer D [50 mM Tris–HCl, pH 7.5, 10 mM $MgCl_2$, 50 mM NaCl], 1 µM δ_2, δ_2K36A or δ_2D60A, 10 µM ATP, 0–2.5 nM *parS* DNA, 0–4.2 µM ω_2 or 1.4 µM ω_2, $\omega_2\Delta$N19 or ω_2T29A and were incubated for up to 180 min at 37°C.

Polymerization of protein δ_2

Dynamic light scattering (DLS) was measured in a 1.5 mm path length quartz cuvette at 90° angle in arbitrary units using a Laser Spectroscatter 201 (RiNA GmbH, Berlin) with 350 nm emission wavelength and plotted using the FL Solutions computer programme and Savitsky-Golay smooth data processing. Aliquots of *Hind*III-linearized 3.1 kb pUC57-borne *parS* DNA (25 nM) were incubated for 2 min on ice with protein δ_2 or variants δ_2K36A or δ_2D60A (1 µM) and different concentrations of ω_2 (0, 0.24, 0.48, 0.96, 1.8 or 3.6 µM) or $\omega_2\Delta$19N (2 µM) in

Table 1. Crystallographic data and refinement statistics

Data statistics	
Beamline	BL14.1 (BESSY)
Wavelength (Å)	0.972
Space group	$P6_522$
Unit cell parameters a, b, c (Å)	83.0, 83.0, 234.0
Resolution range (Å)[a]	50.0–1.83 (1.89–1.83)
No. of observations	400,760
No. of unique reflections	42,966
$I/\sigma I$	11.8 (3.9)
Completeness (%)	99.9 (86.3)
Redundancy	9.2 (8.1)
R_{merge} (%)[b]	6.5 (39.6)
Refinement statistics	
Resolution range (Å)	28.5–1.83 (1.87–1.83)
Reflections in work set	40 877 (2886)
Reflections in R_{free} set	2054 (156)
Residues (atoms)	284 (2313)
Water molecules	256
R_{work}, R_{free}	19.2 (25.0), 21.8 (29.5)
rms deviations[c]	
bond lengths (Å)	0.013
bond angles (°)	1.34
Ramachandran[d]	94.3, 0.4
PDB ID[e]	2OZE

[a]Values in parentheses refer to the outer resolution shell.
[b]$R_{merge} = \sum_{hkl}|I - \langle I\rangle|/\sum_{hkl} I$, where I is the intensity of unique reflection hkl, and $\langle I\rangle$ is the average over symmetry-related observation of unique reflection hkl.
[c]Computed with Procheck (48) also used to determine: [d]The percentage of residues in the 'most favored' regions of the Ramachandran plot and percentage of 'allowed regions', respectively.
[e]Coordinates and structure factors were deposited with the protein data bank (PDB).

buffer E (50 mM Tris-HCl, pH 7.5, 1 mM $MgCl_2$, 1 mM DTE, 5% glycerol). After pre-incubation of the protein•DNA complex for 1 min, ATP, ADP or ATPγS was added to 1 mM final concentration and light scattering was measured as above at 30 s intervals for 5 min and subsequently every 2 min at room temperature. The measured intensity or count rate was the amount of scattered light expressed as photons detected per second and converted to particle size using the Stokes–Einstein relation. The intensity is given in arbitrary units (AU).

Filament formation of protein δ_2 or variants δ_2K36A or δ_2D60A (1 μM) in the absence or presence of fixed (1 μM) or variable concentrations of ω_2, *parS* DNA or ATP•Mg^{2+} was measured in a 1 cm path length quartz cuvette as the change in turbidity using a Hitachi F2500 scanning fluorometer equipped with a thermo-cuvette holder at constant temperature (37°C). Relative light scattering intensities were recorded. Linear 3.1 kb pUC57-borne *parS* DNA (25 nM) was pre-incubated with protein δ_2 (1.2 μM) and different ω_2 concentrations (0, 0.24, 0.48, 0.96, 1.8 or 3.6 μM) in buffer E for 1 min at 37°C. Then, ATP was added to 1 mM final concentration, and the samples were used for light scattering. In presence or absence of linear pUC57-borne *parS* DNA (2 nM), wt δ_2 or variants δ_2K36A or δ_2D60A (1 μM) and ω_2 (1 μM) were pre-incubated in buffer E for 1 min at 37°C. The ATP was added to a 1 mM final concentration and the samples were used for light scattering.

Fluorescence and electron microscopy

Aliquots of *B. subtilis* cultures grown overnight in LB medium at 30°C were diluted in fresh medium to OD_{560} ~0.05. IPTG (10 μM final concentration) was added to OD_{560} ~0.2 cultures to induce the synthesis of $(\delta\text{-GFP})_2$ or $(\delta K36A\text{-GFP})_2$, and incubation was continued until OD_{560} ~0.6. Samples of the cells present were fixed and visualized as described (25). Images were acquired using an Olympus BX61 fluorescence microscope with an Olympus DP70 color CCD camera. Z-stacks of 20–25 images, separated by 0.1 μm, were collected and image deconvolution was performed using Huygens Professional software (Scientific Volume Imaging). DNA was stained using 0.2 μg DAPI/ml before microscopy.

*Eco*RI-linearized 3.1 kb pCB30 or pUC57 DNA (2 nM) harboring *parS* DNA was incubated with the desired protein(s) (see figure legends) for 15 min at 37°C in buffers D or E, respectively, in the presence or absence of 1 mM ATP, as previously described (26). The DNA–protein complexes were visualized by electron microscopy (EM) after negative staining with 1% uranyl acetate (27) or after fixation with 0.2% (v/v) glutaraldehyde for 10 min at room temperature. The procedures for adsorption of the complexes to mica, rotational shadowing with platinum and EM image evaluation have been described previously (28).

RESULTS

Crystal structure of $(\delta\bullet ATP\gamma S\bullet Mg^{2+})_2$

The crystal structure of δ_2 bound to the non-hydrolyzable ATP analogue ATPγS and Mg^{2+} was determined using the structure of the *Tth*Soj monomer in molecular replacement. The crystal asymmetric unit contains one $\delta\bullet ATP\gamma S\bullet Mg^{2+}$ complex that forms a dimer $(\delta\bullet ATP\gamma S\bullet Mg^{2+})_2$ with the two subunits related by a crystallographic *C2* axis (Figure 2A and B). The dimer is stabilized by a hydrophobic surface patch that buries 2197 $Å^2$ of otherwise solvent accessible surface area per subunit, augmented by two reciprocal inter-subunit salt bridges formed between R119 and D189 of each monomer. The structure, refined at 1.83 Å resolution, includes all 284 residues of the wt protein δ. The recombinant version of this protein that was also used in genetic assays (δ_{+14}, Table S1 in the Supplementary Data) carries additional 14 residues at the N-terminus that are disordered in the crystal structure (Table 1).

Gel filtration and chemical cross-linking (Figure S2) confirmed that δ_2 and the Walker A mutant δ_2K36A (see below) form dimers in solution even in the absence of a nucleotide or the presence of ADP.

The δ monomer contains an eight stranded β-sheet surrounded by 12 α-helices (Figure 2A). The N-terminal α-helix (α1) is not conserved in other Walker-box ATPases and shields the outward facing edge of the β-sheet (Figure 2B). The $(\delta\bullet ATP\gamma S\bullet Mg^{2+})_2$ complex is U-shaped and each arm of the U represents one subunit with an ATP-binding site occupied by ATPγS facing the cleft of the U (Figure 2A and B).

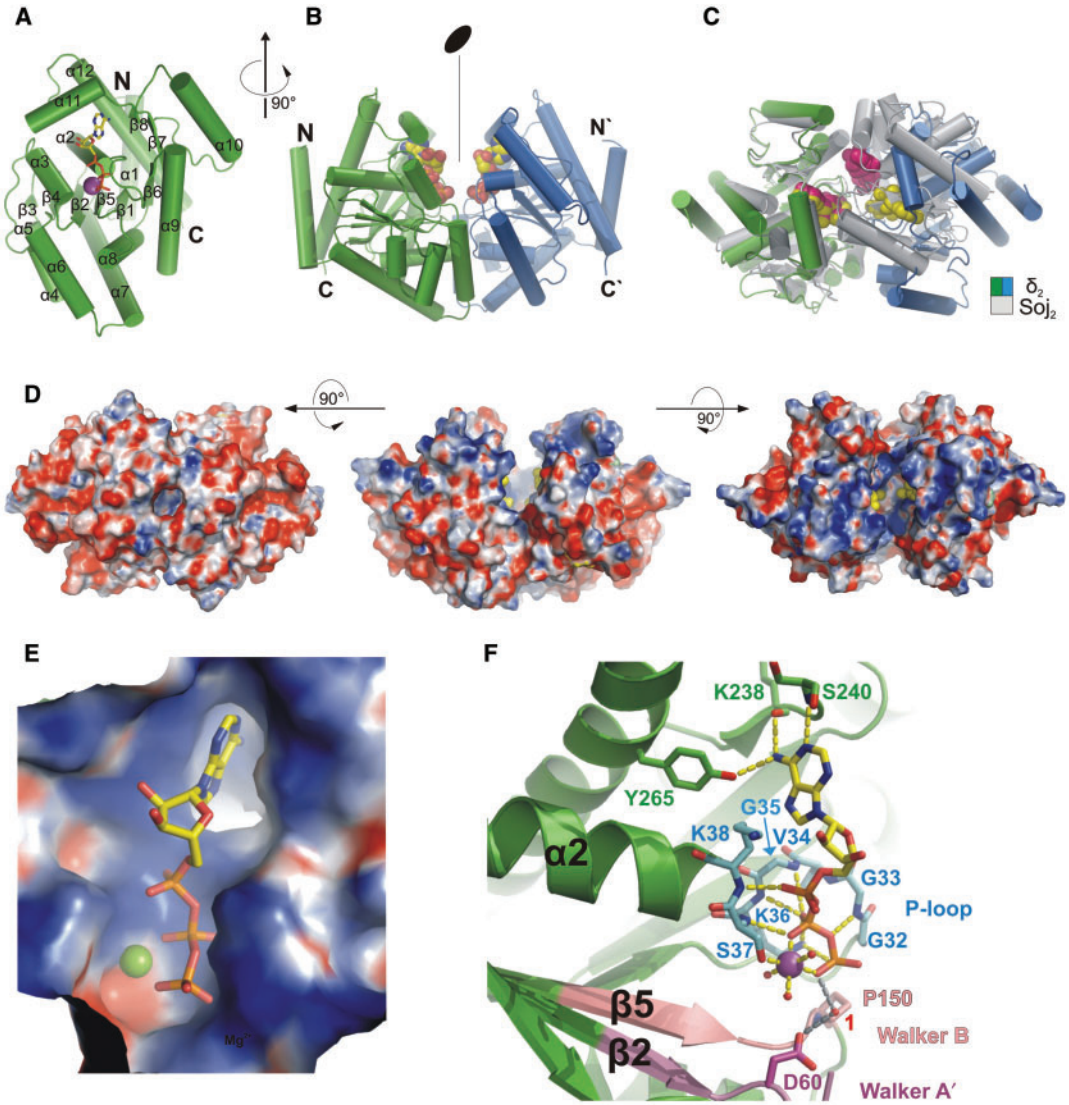

Figure 2. Structure of the $(\delta\bullet ATP\gamma S\bullet Mg^{2+})_2$ complex. (**A**) Structure of a δ monomer with α-helices and β-strands shown as cylinders and arrows, respectively, and labelled sequentially. ATPγS in sticks and Mg^{2+} as a purple sphere, N- and C-termini labelled. (**B**) The monomer shown in (A) is rotated by 90° about the vertical axis (black arrow) and forms $(\delta\bullet ATP\gamma S\bullet Mg^{2+})_2$ with the second monomer shown in blue. ATPγS molecules as CPK models. A twofold crystallographic *C*2 axis (black vertical line with oval) relates both subunits in the crystal structure. (**C**) Superimposition of $(\delta\bullet ATP\gamma S\bullet Mg^{2+})_2$ (green/blue) with (*Tth* SojD44A•ATPγS•$Mg^{2+})_2$ (gray), viewed along the *C*2 axis. The monomers on the left were superimposed and the monomers on the right moved accordingly. (**D**) Electrostatic potential surface representation of $(\delta\bullet ATP\gamma S\bullet Mg^{2+})_2$. The bottom of the U-shaped dimer is negatively charged (left), whereas the upper tips are positively charged (right). (**E**) Electrostatic potential of the nucleotide binding pocket surface with bound ATPγS and Mg^{2+} (green sphere). (**F**) Active site of $(\delta\bullet ATP\gamma S\bullet Mg^{2+})_2$ with the secondary structure elements indicated, hydrogen bonds drawn as yellow dashed lines and octahedrally coordinated Mg^{2+} as a magenta sphere. Lys36 and Asp60 that were substituted by Ala are labelled, water molecules as small red spheres, the water (labelled 1 near P150) is supposed to hydrolyze ATP.

The surface charge of $(\delta\bullet ATP\gamma S\bullet Mg^{2+})_2$ is negative near the bottom of the U and positive at the tips of the arms of the U (Figure 2D). The tip regions therefore most likely bind DNA and/or the negatively charged 'bottom' region of an adjacent δ_2 when assembled into a δ_2 polymer (see below).

The closest structural relatives of the δ monomer structure are *Tth*Soj and *Pfu*MinD although the underlying primary sequences exhibit only 25 and 14% identity, respectively (Figure S1 in the Supplementary Data). Superimposition of δ with 232 Cα atoms of *Tth*Soj and 219 Cα atoms of *Pfu*MinD shows root mean square deviations of 2.2 Å and 3.2 Å, respectively, indicating a high degree of structural similarity between these proteins. However, the structure of the dimer $(\delta\bullet ATP\gamma S\bullet Mg^{2+})_2$ is significantly different from the hydrolysis-deficient $(Tth\text{SojD44A}\bullet ATP\bullet Mg^{2+})_2$ variant.

*Tth*Soj and *Pfu*MinD dimerize only in the presence of ATP. In the dimers, each ATP molecule interacts with both monomers and becomes completely buried within the dimer interface (7,29). Based on these structures, it appears that ADP could only be released after dissociation of $(Tth\text{Soj})_2$ or $(Pfu\text{MinD})_2$ into monomers, whereas the wide and open cleft in the U-shaped $(\delta\bullet ATP\gamma S\bullet Mg^{2+})_2$ allows free exchange of ATP and ADP without dissociation of the subunits.

The nucleotide-binding site

The ATP-binding sites in δ_2 are positively charged (Figure 2E). The adenine N1 and amino group N6 of the two ATPγS form hydrogen bonds to S240Oγ and Y265Oη/K238O, respectively (Figure 2F). The C2′-endo puckered ribose is not engaged in hydrogen bonds but K36-S37-K38 within the Walker A motif at the N-terminus of helix α2 hydrogen bond with their peptide NH groups to α- and β-phosphates of ATPγS, whereas K36Nη forms salt bridges with the β- and γ-phosphates. Mg^{2+} is octahedrally coordinated by β- and γ-phosphate oxygen atoms, by S37Oγ and by three water molecules (Figure 2E and F).

ATP hydrolysis requires a catalytic water molecule (W_{cat}) positioned in-line with the Pγ-Oβ bond ($W_{cat}\cdots$Pγ-Oβ). In Walker-type ATPases, this W_{cat} is activated for nucleophilic attack on the γ-phosphate by an amino acid side chain in the Walker B motif that acts as catalytic base. However, in $(\delta\bullet ATP\gamma S\bullet Mg^{2+})_2$, the position expected for W_{cat} is occupied by P150 within the Walker B motif (Figure 2F) but D60 of the Walker A′ motif hydrogen bonds to and likely activates W_{cat}, which may in turn attack the γ-phosphate group of ATP (Figure 2F). This atypical positioning of amino acids likely participating in catalysis explains the relatively low ATPase activity of δ_2 (see below).

The two above mentioned residues K36 and D60 (Figure S1) were considered to be engaged in the ATPase activity and replaced by Alanine to form δ_2K36A and δ_2D60A (see below).

The ATPase activity of δ_2 is fine-tuned by ω_2 levels in the presence of *parS* DNA and ATP

Since δ_2, ω_2 and *cis*-acting *parS* DNA interact and regulate pSM19035 segregation (see below), we investigated how the presence or absence of ω_2 and/or *parS* DNA affect the enzymatic activity of δ_2. Only experiments with *parS*2 DNA are described here because similar results were obtained with *parS*1 or *parS*3 DNA (Figure 1). The ATPase activity of δ_2 was low and ω_2 had no ATPase activity (Figure 3A). The ATPase activity of δ_2 was not stimulated by the addition of *parS* DNA ($\delta_2 + parS$, Figure 3A). Addition of stoichiometric amounts of ω_2 stimulated the ATPase activity of δ_2 by about 50% ($\delta_2 + \omega_2$; Figure 3A). However, supplementation of *parS* DNA ($\delta_2 + \omega_2 + parS$) resulted in a 3–4-fold stimulation of the ATPase activity of δ_2, which was reduced to ~2-fold when non-*parS* DNA was added ($\delta_2 + \omega_2 +$ non-*parS*, Figure 3A). However, when ω_2 was added at nanomolar concentrations, the ATPase activity of δ_2 was only stimulated by *parS* DNA (Figure 3C, see below).

Stimulation of the ATPase activity of δ_2 was marginal when ω_2 was replaced by ω_2T29A or $\omega_2\Delta$N19 ($\delta_2 + \omega_2\Delta N19 + parS$; $\delta_2 + \omega_2 T29A + parS$, Figure 3B). The ATPase activity of variants δ_2K36A or δ_2D60A amounted to ~30% of wt δ_2 activity and no stimulation of their ATPase activity was observed in the presence of ω_2 and *parS* DNA ($\delta_2 K36A + \omega_2 + parS$ or $\delta_2 D60A + \omega_2 + parS$) (Figure 3B).

The stimulatory effect of increasing ω_2 concentrations on the ATPase activity of δ_2 in the presence of *parS* or non-*parS* DNA was also assayed (Figure 3C). In the presence of *parS* DNA and $\omega_2 : \delta_2$ molar ratios from 0.09:1 to 1.4 : 1 the δ_2-catalyzed ATP hydrolysis was stimulated with the peak around 1.4 μM ω_2, and the stimulation declined when the $\omega_2 : \delta_2$ ratio was further increased from 1.4 : 1 to 4.2 : 1 (Figure 3C). The observed characteristics of ATPase activity stimulation and alleviation of δ_2 is genuinely associated with ω_2 and *parS* DNA. In contrast, when *parS* DNA was replaced by non-*parS* DNA, increasing ω_2 concentrations stimulated the ATPase activity of δ_2 almost linearly (Figure 3C).

Pairing of *parS* regions by proteins ω_2 and δ_2

The complexes formed by δ_2 and *parS* DNA, in the absence or presence of ω_2, $\omega_2\Delta$N19 or ω_2T29A, were visualized by EM at low protein concentrations (Figure 4B–D). The substrate was the linear 3.1-kb pCB30 DNA containing *parS* DNA located at 320 bp from one end (Figure 4A). In presence of $ATP\bullet Mg^{+2}$, δ_2 (100 nM) assembled to form discrete clusters on ~85% of the DNA molecules ($n = 200$) at random locations (Figure 4B), whereas ~40% of the DNA molecules ($n = 250$) that were incubated only with ω_2 showed clusters of ω_2 bound to *parS* on the plasmid (Figure 4C). The *parS* DNA region on linear DNA was not significantly distorted by ω_2 binding, consistent with the prediction based on crystal structures that protein ω_2 would wrap around *parS* sites without significantly bending the DNA double helix [(21), Figure 1C].

At 100 nM ω_2 and 1 nM *parS* DNA but in the absence of $(\delta\bullet ATP\bullet Mg^{2+})_2$ only ~1% of the $\omega_2\bullet$DNA complexes ($n = 300$) contained two DNA molecules that were paired at the position where ω_2 was bound at the *parS* region. The frequency of these complexes was not increased by raising the ω_2 concentration. However, when 1 nM *par*S containing DNA was incubated with 100 nM δ_2, 60 nM ω_2 and 1mM $ATP\bullet Mg^{2+}$, ~20% of the *parS* DNA molecules were paired with DNA molecules juxtaposed at their $\omega_2\bullet parS$ regions ($n = 200$, Figure 4D), indicating that $(\delta\bullet ATP\bullet Mg^{2+})_2$ is required for plasmid pairing (Figure S4A). Plasmid pairing was absent at a 2 : 1 $\omega_2 : \delta_2$ molar ratio (Figure S4B). Replacing ω_2 with $\omega_2\Delta$N19 or ω_2T29A or δ_2 with ω_2K36A abolished DNA pairing (Figure S4C–S4E).

δ_2 polymerization on *parS* DNA is dependent on ω_2 and ATP

DLS data in Figure 5A show that $(\delta\bullet ATP\bullet Mg^{2+})_2$ (1 μM) polymerizes onto linear 3.1-kb *parS* DNA in the presence of a 2 : 1 molar ratio of $\omega_2 : \delta_2$. No δ_2 polymers were formed when either *parS* DNA was omitted (see below), protein ω_2 was substituted by $\omega_2\Delta$N19, or ATP was substituted by ADP (Figure 5A).

ATP binding but no hydrolysis is required for δ_2 polymerization on *parS* DNA in the presence of ω_2 because ATPγS satisfied the cofactor requirement (Figure 5A). In presence of ATP or ATPγS, the size increment of the polymers showed a sigmoidal pattern consistent with cooperative polymerization and levelled off after ~60 min at room temperature. It remained at this level in the presence of ATPγS (Figure 5A, blue line) contrasting the presence of ATP, where polymerization decreased to initial

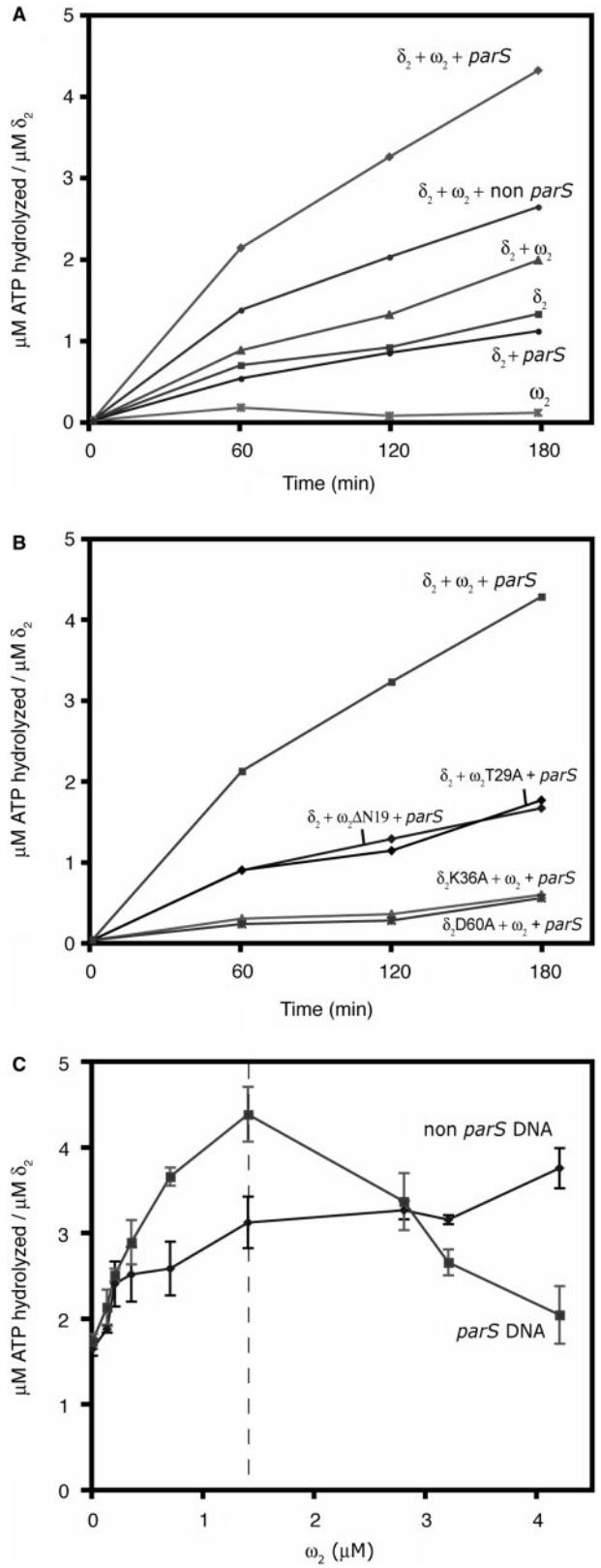

Figure 3. Stimulation of the ATPase activity of δ_2 by ω_2 and DNA. (**A**) ATPase activity in reaction mixtures containing 1 μM δ_2 alone or with 2.5 nM *parS* DNA ($\delta_2 + parS$) or 1.4 μM ω_2 alone or after incubation of 1 μM δ_2 and 1.4 μM ω_2 ($\delta_2 + \omega_2$) or additionally with *parS* DNA ($\delta_2 + \omega_2 + parS$) (average of five experiments, $n = 5$) or with non-cognate DNA ($\delta_2 + \omega_2 +$ non *parS*) ($n = 4$). (**B**) ATPase activity of δ_2 after incubation of 1 μM δ_2 and 1.4 μM $\omega_2\Delta$N19 or ω_2T29A with 2.5 nM *parS* DNA ($\delta_2 + \omega_2$T29A + *parS*) or ($\delta_2 + \omega_2\Delta$N19 + *parS*), or after incubation of 1 μM δ_2K36A or δ_2D60A and 1.4 μM ω_2 with 2.5 nM *parS* DNA (δ_2K36A + ω_2 + *parS*) or (δ_2D60A + ω_2 + *parS*). (**C**) ATPase activity of 1 μM δ_2 when incubated with increasing ω_2 concentrations (0.09–4.2 μM) and 2.5 nM *parS*2 DNA or non-cognate (non *parS*) DNA at 37°C. Values are averages of more than four independent experiments.

values after ~90 min (Figure 5A, red line), indicating that ATP hydrolysis induces depolymerization, and the formed $(\delta\bullet ADP\bullet Mg^{2+})_2$ complex did not support the integrity of the polymer. When fresh ATP was added to this solution after 120 min, δ_2 polymerized again in a new cycle (data not shown). This indicates that the binding of ATP to δ_2 enhances high affinity DNA binding (Table S2), and interaction of $(\delta\bullet ATP\bullet Mg^{2+})_2$ with $\omega_2\bullet$parS DNA leads to δ_2 polymerization onto DNA, whereas ATP hydrolysis induced depolymerization. This is consistent with the observation, using atomic force microscopy, that no ω_2 nucleoprotein filaments are formed onto linear or supercoiled *parS* DNA in the absence of $(\delta\bullet ATP\bullet Mg^{2+})_2$ (F.P., K. Takeyasu and J.C.A., unpublished results).

EM revealed that $(\delta\bullet ATP\bullet Mg^{2+})_2$ (1 μM) assembled and polymerized along the full-length of linear 3.1-kb *parS*-containing DNA molecules in presence of saturating amounts of ω_2 (1 μM) (Figure S3A). However, such polymers were not observed when ATP was omitted (Figure S3B). The estimated protein volume of the nucleoprotein filament was only compatible with δ_2 polymerization on DNA. Indeed, the molecular mass of δ_2 is 4.3-fold larger than that the one of ω_2 (the molecular masses are 68.8 and 15.9 kDa, respectively) (11,15).

Protein $(\delta\bullet ATP\bullet Mg^{2+})_2$ polymerizes rapidly on *parS* DNA in the presence of an excess of ω_2 at 37°C. However, no $(\delta\bullet ATP\bullet Mg^{2+})_2$ polymers formed on *parS* DNA when the $\omega_2 : \delta_2$ molar ratio was 0.2 : 1 or below, suggesting that a minimal concentration of ω_2 is needed under the experimental conditions used (Figure 5B). The extent of δ_2 polymerization onto DNA increased with ω_2 concentrations, because the light scattering signal was lower at $\omega_2 : \delta_2$ ratios of 0.75 : 1 compared to $\omega_2 : \delta_2$ molar ratios of 1.5 : 1 to 3 : 1 (black and blue lines; Figure 5B). Alternatively, at high $\omega_2 : \delta_2$ ratios, the elevated ω_2 concentrations promoted δ_2 polymerization even onto non-*parS* DNA.

Using 90° light scattering, we investigated the component requirements for δ_2 polymerization (Figure 5C). In presence of ATP, no polymerization was observed when ω_2 $[(\delta\bullet ATP\bullet Mg^{2+})_2 + parS]$ or *parS* DNA $[(\delta\bullet ATP\bullet Mg^{2+})_2 + \omega_2]$ were omitted or in presence of ATPγS when protein ω_2 was omitted ($\delta_2 + parS + ATP\gamma S$) (Figure 5C), suggesting that δ_2 polymerization on DNA requires the interaction with ω_2. To further evaluate the effect of the nucleotide cofactor, the δ_2D60A and δ_2K36A variants were also analyzed. As shown in Table S2, protein δ_2 or δ_2D60A bound with ~12-fold higher affinity to *parS* DNA in the presence of ATP than ADP, while binding of δ_2K36A to *par*S DNA was weak, regardless of the presence of ATP or ADP. Wild type δ_2 and variant δ_2D60A feature similar polymerization kinetics ($\delta_2 + \omega_2 + parS$ *vs* δ_2D60A + $\omega_2 + parS$) (Figure 5C), albeit the equilibrium was reached earlier in case of δ_2D60A and the formed filaments were shorter. In contrast, variant δ_2K36A showed

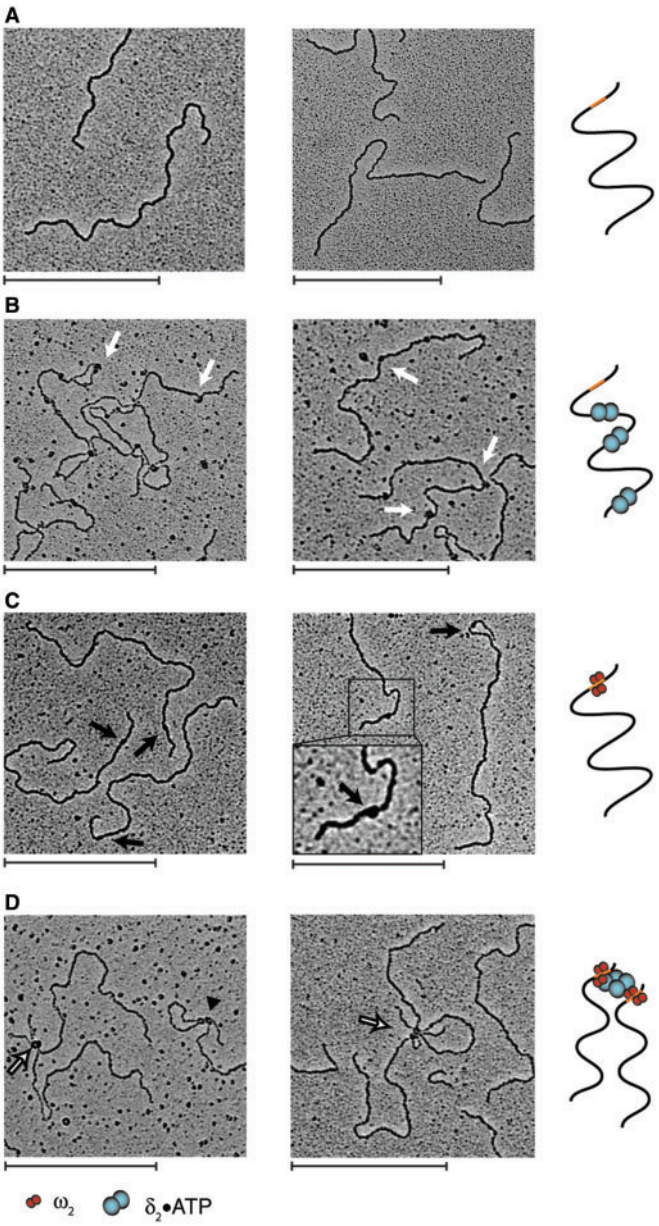

Figure 4. Electron micrographs of protein•DNA complexes. In the illustrated cartoons *parS* DNA, located 320 bp from one end (orange) of 3.1-kb linear pCB30 DNA, was incubated with ω_2 (red spheres) and/or δ_2 (blue spheres), in the presence of 1 mM ATP and the complexes formed were visualized by EM. Linear DNA (1 nM) alone (**A**), plus δ_2 (100 nM) (white arrows) (**B**), plus ω_2 (60 nM), showing ω_2•*parS* complexes (black arrows) (**C**). (**D**) Linear *parS* DNA (1 nM) incubated with δ_2 (100 nM) and ω_2 (60 nM) in the presence of 1 mM ATP with paired molecules indicated by empty arrows. The bars indicate 500 nm.

a near-linear increase in light scattering or slowly assembled on *parS* DNA in the presence of ω_2 and ATP (δ_2K36A + ω_2+ *par*S; Figure 5C).

Plasmid segregation requires (δ•ATP•Mg^{2+})$_2$, ω_2 and *parS* DNA

To test the importance of proteins ω_2 and δ_2 and a *cis*-acting *parS* site for plasmid segregation, we combined the respective genes and variants in the rolling-circle replicating and segregationally unstable vector pHP13 (Table S1). This vector was reported to replicate far from mid-cell and its replication imposes a metabolic burden that compromises its maintenance in host cells (30). The frequency of plasmid-loss was measured in *B. subtilis* cultured in LB medium at 30°C. Plasmids bearing a *parS*1 site and genes that directed the synthesis of ω_2 and δ_2 (pCB706) or ω_2 and (δ-GFP)$_2$ (δ_2 with C-terminally fused GFP, pCB702) were retained in progeny cells at ~10-fold higher frequencies (Table S3) than predicted if the plasmid were randomly distributed (see Materials and methods section). However, random distribution was observed if plasmids lacked either the ω or δ gene or carried genes that encoded variants δK36A, ωΔN19 or ωT29A (Table S3). This indicates that the integrity of the ATP binding site of δ_2, DNA binding and the N-terminus of ω_2 and *parS* DNA are essential for correct pSM19035 partitioning.

Dynamic movement of protein (δ-GFP)$_2$ depends on *parS* DNA and ω_2

To gain insight into the molecular mechanism by which the fully functional (δ-GFP)$_2$ (see above) contributes to plasmid segregation, we imaged its cellular localization in the presence or absence of ω_2. The GFP signal overlapped with that of DAPI-stained DNA in 90% of the cells of a *B. subtilis* strain containing a pCB578-borne δ-*gfp* gene transcribed from its own P_δ (*parS*1) promoter (Figure 6). When ω_2 was also present (pCB702) it repressed the δ-GFP synthesis by ~70-fold compared to the absence of ω_2 (15). The low (δ-GFP)$_2$ signal was no longer statically associated with the nucleoid but was dynamically located near the cell poles and/or associated with the nucleoid. Image deconvolution showed that in the presence of *parS* DNA, ω_2 and (δ-GFP)$_2$ a spiral-like structure was formed within the cytosol of *B. subtilis* cells (Figure 6B). It is of interest that unlike (δ-GFP)$_2$ that only formed a spiral-like structure in presence of *parS* DNA and ω_2 under auto-regulated conditions, spiral-shaped filaments formed by other ParA (pB171-ParA or F-SopA) neither required ParB (pB171-ParB or F-SopB) nor *parS* (pB171-*parC* or F-*sopC*) DNA (31,32).

To vary the intracellular concentration of (δ-GFP)$_2$ independently of the ω_2 concentration, we placed the δ-*gfp* gene under the transcriptional control of the LacI repressor and integrated a single copy of this construct into the *amy* locus of the *B. subtilis* genome (Figure 7A). In the absence of a plasmid-borne *parS* site and of gene ω, (δ-GFP)$_2$ was seen to co-localize at low IPTG concentration (10 μM) with the nucleoid in ~90% of the cells (n = 300), suggesting that (δ-GFP)$_2$ binds non-specifically to DNA (Figure 7B and 7B′) and the fluorescence signal of (δ-GFP)$_2$ was 2- to 3-fold higher than the one from cells bearing the pCB578-borne *parS*1 site and gene δ-*gfp* (Table S1). Under this condition, the presence of a *parS* region and ω_2 led to (δ-GFP)$_2$ re-localization ('oscillation') near one cell pole in ~60% of the cells (n = 300) that had one nucleoid, or co-localized with one nucleoid in ~70% of the cells (n = 200) that had two nucleoids (Figure 7C and 7C′). Similar results were reported for the chromosomally encoded *Bsu*Soj in the presence of *Bsu*Spo0J and *parS* sites (25,33).

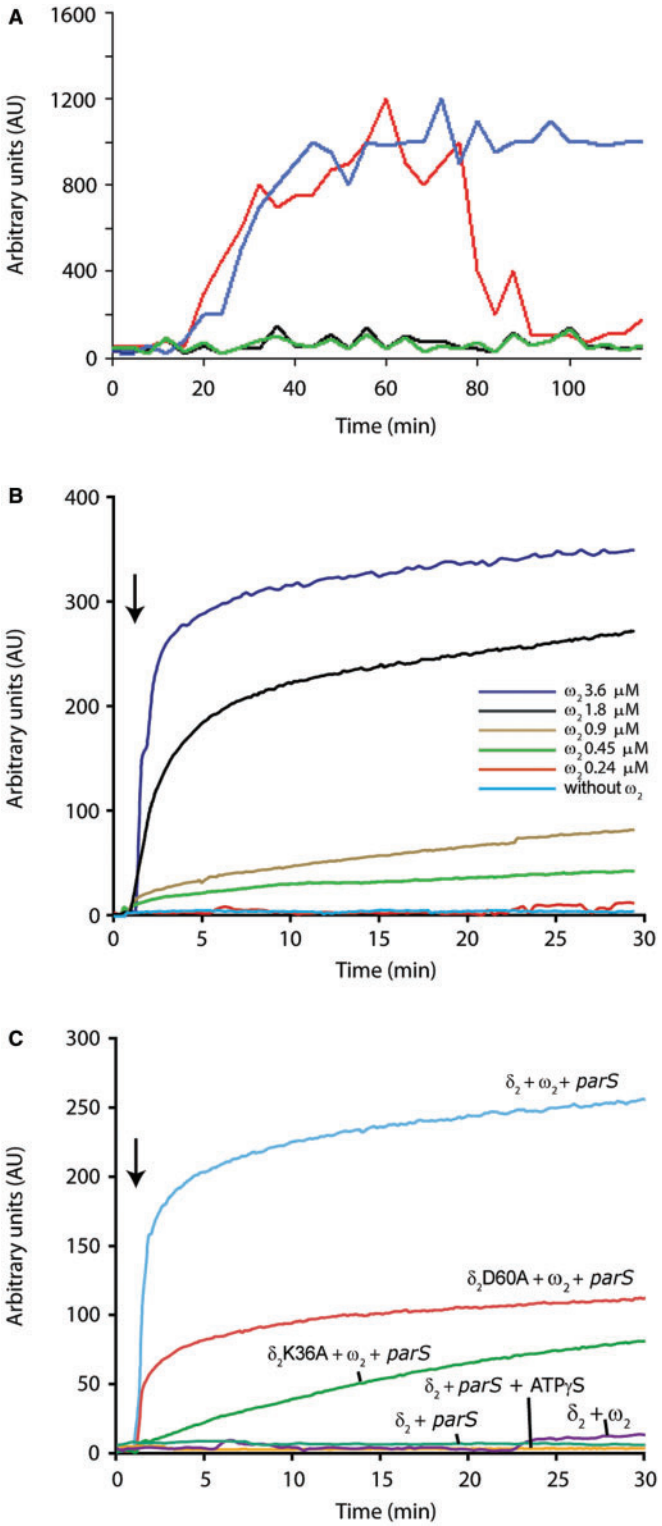

Figure 5. Polymerization of δ_2 in the presence of *parS* DNA, ω_2 or $\omega_2\Delta$N19 and ATP, ADP or ATPγS. (**A**) Dependence of light scattering (AU) on time (min). Reaction mixtures containing linear 3.1-kb *parS* DNA (20 nM), 1 μM δ_2 and 2 μM ω_2 or $\omega_2\Delta$N19 proteins were pre-incubated on ice in buffer E and DLS was measured at room temperature. At time zero, we added 1 mM of ATP to δ_2 and ω_2 (red line) and to δ_2 and $\omega_2\Delta$N19 (green line), 1 mM ATPγS to δ_2 and ω_2 (blue line) or 1 mM ADP to δ_2 and ω_2 (black line). (**B**) Light scattering increases with increasing $\omega_2:\delta_2$ ratio. Reaction mixtures containing 3.1-kb *parS* DNA (20 nM), 1.2 μM δ_2 and the indicated ω_2 concentration were pre-incubated at 37°C in buffer E. Polymerization was initiated by the addition of 1 mM ATP (denoted by an arrow). Light scattering was measured at 37°C. Values are averages of three independent experiments. (**C**) Polymerization of protein δ_2 requires ω_2, *parS* DNA and ATP•Mg^{2+}, as shown by an increase of light scattering. Reaction mixtures containing 3.1-kb *parS* DNA (20 nM), 1 μM δ_2, δ_2D60A or δ_2K36A and 2 μM ω_2 were pre-incubated at 37°C in buffer E. Polymerization was initiated by the addition of 1 mM ATP (denoted by an arrow). Light scattering was measured at 37°C. Values are averages of four independent experiments.

When ω_2 was replaced by $\omega_2\Delta$N19 (Figure 7D and 7D′) or by ω_2T29A (data not shown), $(\delta\text{-GFP})_2$ co-localized with the nucleoid both in the presence or absence of *parS* DNA. Since $\omega_2\Delta$N19 binds to *parS* as well as wt ω_2, contrasting ω_2T29A that does not specifically bind to *parS* DNA (18,19,21), this shows that not only the ability of ω_2 to bind *parS*, but the N-terminal region of ω_2 is also required to stimulate the redistribution of $(\delta\text{-GFP})_2$ from the nucleoid to the cell poles.

At levels comparable to $(\delta\text{-GFP})_2$, the $(\delta$K36A-GFP$)_2$ signal was distributed throughout the cells regardless of the presence or absence of a *parS* sequence and/or gene ω (Figure 7E, 7E′, 7F and 7F′). This indicates that the binding of δ_2 to DNA and oscillation in the cell requires ATPase activity. Indeed, variant $(\delta$K36A-GFP$)_2$ bound to *parS* or non-*parS* DNA with a 6- to 7-fold lower affinity than wt δ_2 (Table S2).

DISCUSSION

ATPase δ_2, structure and properties

We showed that the ATPase δ_2 from the Firmicute plasmid pSM19035 and *Eco*MinD and *Tth*Soj from Gram-negative bacteria have similar monomer structures, but form dimers under different conditions. *Eco*MinD and *Tth*Soj are monomers in solution with or without ADP•Mg^{2+}, and binding of ATP•Mg^{2+} induces formation of structurally similar dimers (7,29). In contrast, δ forms a dimer regardless of the presence of ADP•Mg^{2+} or ATP•Mg^{2+} or absence of a nucleotide cofactor (Figure S2) that is structurally different from the above two dimers (Figure 2B).

The ATPase activity of δ_2 is regulated by binding of the ω_2•*parS* DNA complex to δ_2. When the concentrations of ω_2 were increased up to 1.4 : 1 $\omega_2:\delta_2$ ratios the ATPase activity was stimulated but above this $\omega_2:\delta_2$ ratio, the stimulation diminished when the concentration of ω_2 is further increased up to a ratio of 4.2 : 1.

Dynamic assembly of $(\delta$•ATP•$Mg^{2+})_2$ on ω_2•*parS*

Our results show that pSM19035-borne *parS* sequence(s), ATP binding and hydrolysis by δ_2, and the N-terminus and the DNA binding ability of ω_2 are essential components of the genuine pSM19035 partition system, because the mutation or deletion of either one of these components abrogates plasmid segregation. Protein $(\delta\text{-GFP})_2$ localized within the nucleoid of *B. subtilis* cells, whereas catalytically inactive $(\delta$K36A-GFP$)_2$ was distributed throughout the cytoplasm, arguing for ATP•Mg^{+2}-dependent nucleoid localization (Figure 7E and F). Under native regulation,

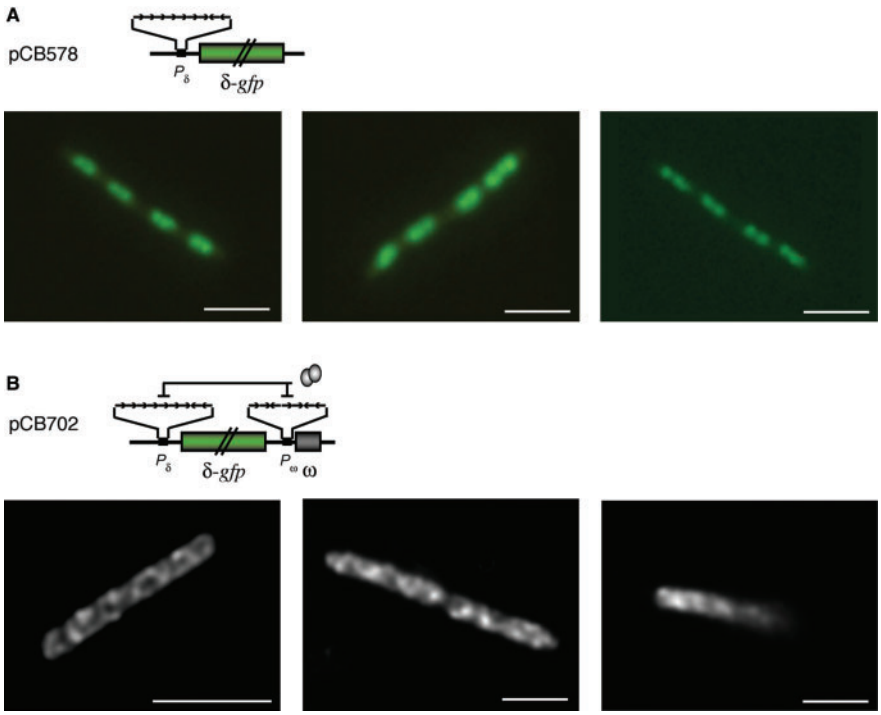

Figure 6. Subcellular localization of $(\delta\text{-GFP})_2$ in the presence or absence of ω_2 and *parS* DNA. (**A**) The top illustration shows the structure of pCB578-borne P_δ (*parS*1) and δ-*gfp* gene in *B. subtilis* cells. The lower panels show the localization of $(\delta\text{-GFP})_2$ fusion protein in the absence of protein ω_2. Bars indicate 2 μm. (**B**) The top illustration shows the structure of pCB702-borne P_δ (*parS*1) and δ-*gfp* gene, P_ω (*parS*2) and ω gene in *B. subtilis* cells, and the repression by protein ω_2 is indicated by ellipsoids. The lower panels show the spiral-like organization of $(\delta\text{-GFP})_2$ fusion protein in the presence of *parS* DNA, $(\delta\text{-GFP})_2$ and ω_2. Images captured in different optical planes were subjected to 2D deconvolution. Bars indicate 2 μm.

$(\delta\text{-GFP}\bullet\text{ATP}\bullet Mg^{+2})_2$, ω_2 and *parS* DNA formed spiral-like structures (Figure 6B) by a mechanism that depends on the integrity of the ATPase activity of $(\delta\text{-GFP})_2$. However, in presence of *parS* DNA, a moderate excess of $(\delta\text{-GFP})_2$ over ω_2 resulted in relocation or oscillation of $(\delta\text{-GFP})_2$ from the nucleoid to the cell poles. It is striking that spiral-like structures were only observed in the presence of $(\delta\text{-GFP})_2$, *parS* DNA and ω_2 under autoregulated conditions. Possibly, the excess $(\delta\text{-GFP})_2$ bound to the nucleoid masked the weak signal of $(\delta\text{-GFP}\bullet\text{ATP}\bullet Mg^{+2})_2$ interacting with $\omega_2\bullet$*parS* on the plasmid DNA only observed under native conditions.

In vivo, spiral-shaped filaments formed by γ proteobacterial plasmids of the ParA-Ia or ParA-Ib families required only ParA (pB171-ParA or F-SopA) (31,32). This apparent paradox between the segregation mechanisms of plasmids of Proteobacteria and Firmicutes can be reconciled if one type of filaments were inactive (representing a storage form) and the other type were the active form. Alternatively, considering that the phylogenic divide between γ Proteobacteria and Firmicutes is large (more than 1.5 billion years), we might assume that the ParA partition systems of these evolutionarily distant bacteria evolved different mechanisms to secure plasmid segregation during cell division.

The catalytic activity of δ_2 is influenced by the concentration of ω_2

Pairing of *parS* sites from two pSM19035 plasmids requires both, $(\delta\bullet\text{ATP}\bullet Mg^{+2})_2$ and ω_2 in the nM range (Figure 4D) to organize a structure that facilitates plasmid segregation. Indeed, the presence of ω_2 alone gave rise to only few (~1%) presumably short-living and/or unstable pairs and failed to promote centromere pairing of pSM19035. Plasmid pairing at *parS* regions was observed at a $\omega_2 : \delta_2$ ratio of 0.6 : 1 (Figure 4D), but no pairing was observed at a $\omega_2 : \delta_2$ ratio of 1.2 : 1 (Figure S4B). The given ω_2 concentration also affects the ATPase activity of δ_2. Molar $\omega_2 : \delta_2$ ratios of 0.09 : 1 to 1.4 : 1 stimulate ATP hydrolysis, whereas higher ratios (2.8 : 1 to 4.2 : 1) have the opposite effect and diminish the δ_2 ATPase activity (Figure 3C). Moreover, we have shown here that the ω_2 concentration needs to exceed a threshold to stimulate/initiate δ_2 nucleoprotein filament formation (Figure 5B). In contrast, *in vitro* pairing of plasmids of the γ Proteobacteria requires only the centromere binding protein (R1-ParR or pB171-ParB) in the μM range and its cognate *parC* site, but is independent of its ParA partner (28,34). This was also observed *in vivo* by supercoil trapping for P1-ParB•*parS* (35).

Formation of nucleoprotein filaments and proteofilaments have different requirements

In vitro, ParA filament formation has a different requirement for plasmids of γ Proteobacteria than those of the Firmicutes phylum. Protein $(\delta\bullet\text{ATP}\bullet Mg^{2+})_2$ of Firmicutes polymerized onto DNA at high $\omega_2 : \delta_2$ ratios, and formed nucleoprotein filaments that in turn depolymerized when ATP was hydrolyzed. When new ATP was added, polymerization was reinitiated (Figure 5A). Filament formation by δ_2 onto DNA was not observed

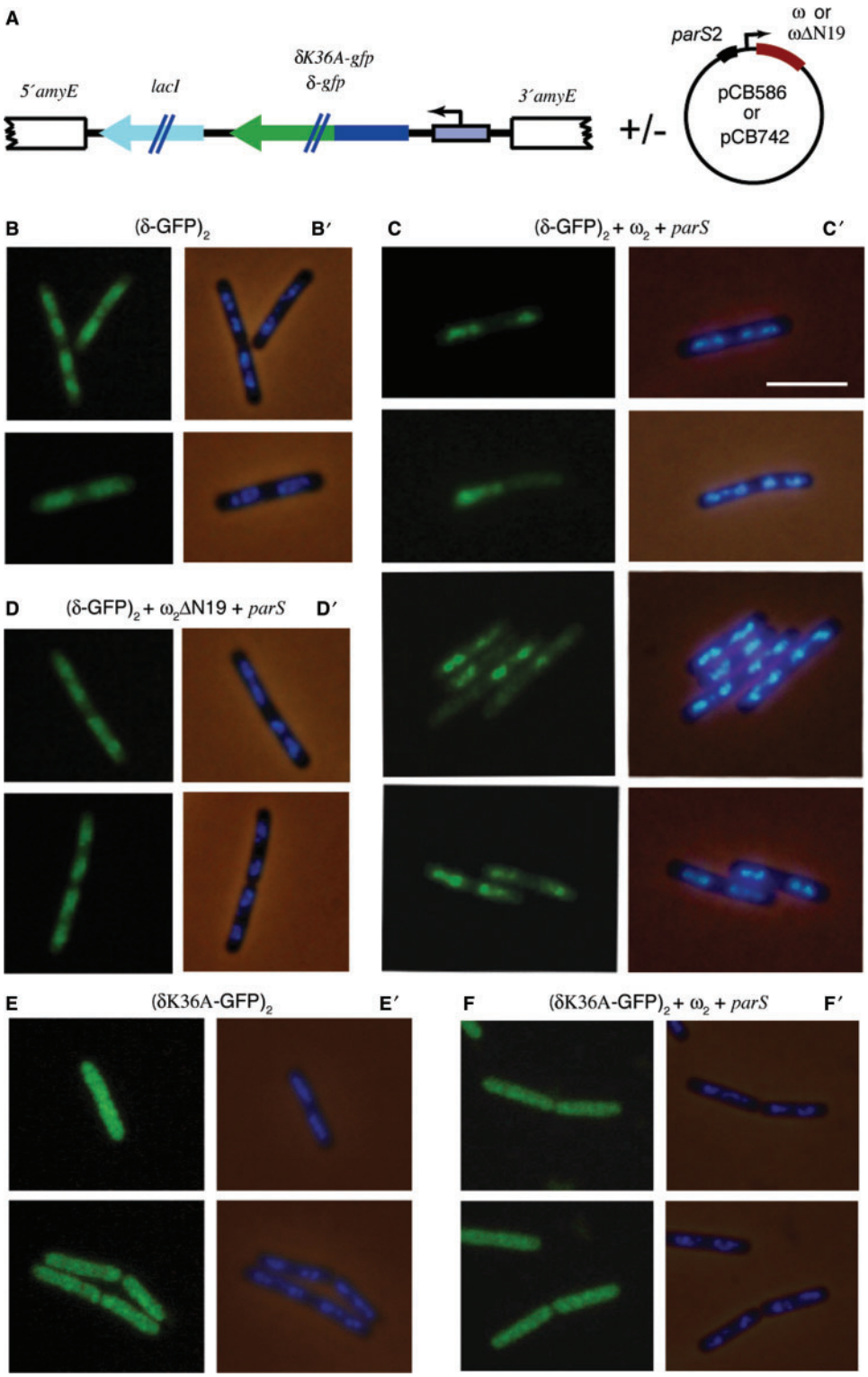

Figure 7. Subcellular localization of $(\delta\text{-GFP})_2$ in *B. subtilis* cells in the presence or absence of *parS* and protein ω_2. (**A**) Illustrations showing the structure of the $(\delta\text{-GFP})_2$ expression cassettes integrated into the *B. subtilis* chromosome, and plasmids that had or lacked a *parS*2 sequence and encoded ω or the ωΔN19 variant. (**B**–**F**) Images of cells with fluorescence from $(\delta\text{-GFP})_2$ or $(\delta\text{K36A-GFP})_2$ and (B′ to F′) images of the same cells stained with DAPI to show DNA. Cells contained $(\delta\text{-GFP})_2$ (B), $(\delta\text{-GFP})_2$, ω_2 and *parS* DNA (C), $(\delta\text{-GFP})_2$, $\omega_2\Delta$N19 and *parS* DNA (D), $(\delta\text{K36A-GFP})_2$ (E) and $(\delta\text{K36A-GFP})_2$, ω_2 and *parS* DNA (F) were taken from exponentially growing cultures in the presence of 10 μM IPTG. Scale bar (in C′) is 2 μm.

when ω_2 or ATP was omitted or when ω_2 was replaced by $\omega_2\Delta$N19. Like protein δ_2, chromosomally encoded *Tth*Soj—from the *Deinococcus-Thermus* phylum—also forms nucleoprotein filaments onto DNA, but does not require its ParB partner Spo0J (29). Recently it was shown that one of the arginine residues (R189 in *Bsu*Soj) that is conserved among chromosome-encoded ParA-Ib type ATPases lies on the surface of the Soj dimer and is essential for binding to DNA (36). In δ_2, the equivalent position features S212 (Figure S1).

Dynamic assembly and disassembly of *Eco*MinD resembles that of δ_2 or the *Tth*Soj systems. *Eco*MinD assembled only on the surface of phospholipid vesicles and formed filaments in the presence of ATP•Mg^{2+} (37). Addition of *Eco*MinE promoted *Eco*MinD disassembly through stimulation of its ATPase activity (37,38).

In vitro, proteofilaments formed by proteobacterial plasmids of the ParA-Ia or ParA-Ib families required only ParA (pB171-ParA or F-SopA) but *neither required ParB* (pB171-ParB or F-sopB) *nor parS* (*parC* or *sopC*) DNA (31,32). Even in the absence of DNA and its ParB partner, purified ParA-Ia or ParA-Ib ATPases of proteobacterial plasmids are stimulated by the addition of ATP and form surface-independent proteofilaments and bundles that continuously increase in length (39–41). Replacement of ATP by ATPγS had different outcomes since it failed to induce polymerization in case of F-SopA but greatly stimulated polymerization in case of pTP228-ParF (40,41).

Modelling ω_2•parS•$(\delta\bullet ATP)_2$ segregation

Many of the models proposed for ParA-type partitioning systems of plasmids isolated from γ Proteobacteria share some features in common with the ParM-type system (9,42,43) because ParB promotes pairing of ParB•*parS* complexes, and ParA forms multi-stranded proteofilaments formed in the absence of ParB and *parS* DNA (32,34,40,41,44,45). There is no evidence for filament disassembly in the presence of their ParB homologs, which markedly stimulate (~30-fold) ATP hydrolysis, and a large excess (>10-fold) of ParB-like protein does not exert a negative effect on the activity of the ParA ATPase (46). These features neither apply for plasmids isolated from Firmicutes nor for chromosome-encoded ParA systems [(5), this work].

On the basis of all our findings with the pSM19035 Par system, we propose a model that is distinct to those developed for Proteobacterial plasmids. In *B. subtilis* cells, the best studied member of the Firmicutes, plasmids move dynamically within the cytosol, and the replisome is recruited to the subcellular position of the plasmid rather than to a central stationary position of the chromosomally associated replisome (30). Replication and segregation of pSM19035 are regulated by the intracellular concentration of ω_2 (15). Upon plasmid replication, ω_2 binds to and wraps around the *parS* sites on pSM19035 DNA to mediate both, transcriptional regulation and segregation [(15,21), Figure 1C]. In an artificial system, which contains only one *parS* site, ω_2 and *parS* form a *parS*•ω_2 complex with only limited extension (spreading) on non-specific sequences (15,17). This complex stimulates the recruitment of $(\delta\bullet ATP\bullet Mg^{2+})_2$, and the resulting *parS*•ω_2•$(\delta\bullet ATP\bullet Mg^{2+})_2$ nucleoprotein super-structure leads to intermolecular pairing of *parS* regions and accurate positioning of plasmid copies. In the natural context, with six consecutive *parS* sites, multiple *parS*•ω_2 complexes can be formed and organized into higher-order complexes.

We postulate that once the plasmids are paired, the local intracellular concentration of ω_2 increases, the ATPase activity of δ_2 decreases, plasmid pairing is lost and polymerization of $(\delta\bullet ATP\bullet Mg^{2+})_2$ onto plasmid DNA is stimulated. Protein $(\delta\bullet ATP\bullet Mg^{2+})_2$ nucleation onto plasmid DNA at the ω_2•*parS* DNA complex, thereby generates one end of the nucleoprotein filament [*parS*•ω_2•$(\delta\bullet ATP\bullet Mg^{2+})_2$]. From this initial assembly site, polymerization of $(\delta\bullet ATP\bullet Mg^{2+})_2$, leads to the formation of a nascent δ_2 filament that depends on the presence of ATP, but is independent of ATP hydrolysis, to reach the end where another *parS*•ω_2•$(\delta\bullet ATP\bullet Mg^{2+})_2$ complex is located. The decrease of the $\omega_2:\delta_2$ molar ratio at the site where the δ_2 filament encounters another *parS*•ω_2 complex will stimulate the ATPase activity of δ_2 (Figure 3A) and after ATP hydrolysis $(\delta\bullet ADP\bullet Mg^{2+})_2$ will dissociate from the nucleoprotein complex, beginning proximal to the ω_2•*parS* region. A *parS*•ω_2 diffusion towards the adjacent $(\delta\bullet ATP\bullet Mg^{2+})_2$ molecule in the nucleoprotein filament can then re-initiate the cycle of ATP hydrolysis and propagation along the DNA lattice towards opposite ends, with subsequent retraction of the δ_2 nucleoprotein filament. The disassembly of filaments could contract the spiral-like structure (Figure 6) by moving the same cargo (individual ω_2•*parS* region) in a step-wise motion, and generate a force that moves the plasmid DNA *outwards* along the cell axis. The proposed model depends on changes in the intracellular concentration of ω_2, the dislodging of δ_2 from the nucleoid and the assembly and disassembly of δ_2 rather than on anchoring of the δ_2 nucleoprotein filament at the cell quarters or at mid-cell (47). Although many questions remain, the data reported here favor pSM19035 pairing before δ_2 nucleoprotein filament dynamics, thereby securing plasmid movement from the replication site to opposite cell poles. A similar mechanism may be employed by some chromosomally encoded partition systems (5).

SUPPLEMENTARY DATA

Supplementary Data are available at NAR Online.

ACKNOWLEDGEMENTS

We thank D. Rudner (Harvard University) for providing plasmid pDR111, C. Böttcher (Freie Universtät Berlin) for help with EM. This work was partially supported by grants BFU2006-01062 from Ministerio de Educación y Ciencia-Dirección General de Investigación (MEC-DGI) to J.C.A. and by EU-grant QLK2-CT-2002-01079 to J.C.A. and W.S. Crystallographic atomic coordinates and structure factors have been deposited with the Protein

Data Bank under accession code 2OZE. Funding to pay the Open Access publication charges for this article was provided by MEC-DGI.

Conflict of interest statement. None declared.

REFERENCES

1. Scholey,J.M., Brust-Mascher,I. and Mogilner,A. (2003) Cell division. *Nature*, **422**, 746–752.
2. Ghosh,S.K., Hajra,S., Paek,A. and Jayaram,M. (2006) Mechanisms for Chromosome and Plasmid Segregation. *Annu. Rev. Biochem.*, **75**, 211–241.
3. Funnell,B.E. (2005) Partition-mediated plasmid pairing. *Plasmid*, **53**, 119–125.
4. Ebersbach,G. and Gerdes,K. (2005) Plasmid segregation mechanisms. *Annu. Rev. Genet.*, **39**, 453–479.
5. Leonard,T.A., Moller-Jensen,J. and Lowe,J. (2005) Towards understanding the molecular basis of bacterial DNA segregation. *Philos. Trans. R. Soc. Lond. B Biol. Sci.*, **360**, 523–535.
6. Larsen,R.A., Cusumano,C., Fujioka,A., Lim-Fong,G., Patterson,P. and Pogliano,J. (2007) Treadmilling of a prokaryotic tubulin-like protein, TubZ, required for plasmid stability in *Bacillus thuringiensis*. *Genes Dev.*, **21**, 1340–1352.
7. Shih,Y.L. and Rothfield,L. (2006) The bacterial cytoskeleton. *Microbiol. Mol. Biol. Rev.*, **70**, 729–754.
8. Hayes,F. and Barilla,D. (2006) The bacterial segrosome: a dynamic nucleoprotein machine for DNA trafficking and segregation. *Nat. Rev. Microbiol.*, **4**, 133–143.
9. Moller-Jensen,J., Ringgaard,S., Mercogliano,C.P., Gerdes,K. and Lowe,J. (2007) Structural analysis of the ParR/parC plasmid partition complex. *EMBO J.*, **26**, 4413–4422.
10. Schumacher,M.A., Glover,T.C., Brzoska,A.J., Jensen,S.O., Dunham,T.D., Skurray,R.A. and Firth,N. (2007) Segrosome structure revealed by a complex of ParR with centromere DNA. *Nature*, **450**, 1268–1271.
11. Ceglowski,P., Boitsov,A., Chai,S. and Alonso,J.C. (1993) Analysis of the stabilization system of pSM19035-derived plasmid pBT233 in *Bacillus subtilis*. *Gene*, **136**, 1–12.
12. Ceglowski,P., Boitsov,A., Karamyan,N., Chai,S. and Alonso,J.C. (1993) Characterization of the effectors required for stable inheritance of *Streptococcus pyogenes* pSM19035-derived plasmids in *Bacillus subtilis*. *Mol. Gen. Genet.*, **241**, 579–585.
13. Ceglowski,P., Lurz,R. and Alonso,J.C. (1993) Functional analysis of pSM19035-derived replicons in *Bacillus subtilis*. *FEMS Microbiol. Lett.*, **109**, 145–150.
14. Ceglowski,P. and Alonso,J.C. (1994) Gene organization of the *Streptococcus pyogenes* plasmid pDB101: sequence analysis of the orf eta-copS region. *Gene*, **145**, 33–39.
15. de la Hoz,A.B., Ayora,S., Sitkiewicz,I., Fernandez,S., Pankiewicz,R., Alonso,J.C. and Ceglowski,P. (2000) Plasmid copy-number control and better-than-random segregation genes of pSM19035 share a common regulator. *Proc. Natl Acad. Sci. USA*, **97**, 728–733.
16. Dmowski,M., Sitkiewicz,I. and Ceglowski,P. (2006) Characterization of a novel partition system encoded by the delta and omega genes from the streptococcal plasmid pSM19035. *J. Bacteriol.*, **188**, 4362–4372.
17. de la Hoz,A.B., Pratto,F., Misselwitz,R., Speck,C., Weihofen,W., Welfle,K., Saenger,W., Welfle,H. and Alonso,J.C. (2004) Recognition of DNA by omega protein from the broad-host range *Streptococcus pyogenes* plasmid pSM19035: analysis of binding to operator DNA with one to four heptad repeats. *Nucleic Acids Res.*, **32**, 3136–3147.
18. Welfle,K., Pratto,F., Misselwitz,R., Behlke,J., Alonso,J.C. and Welfle,H. (2005) Role of the N-terminal region and of β-sheet residue Thr29 on the activity of the ω_2 global regulator from the broad-host range *Streptococcus pyogenes* plasmid pSM19035. *Biol. Chem.*, **386**, 881–894.
19. Dostál,L., Pratto,F., Alonso,J.C. and Welfle,H. (2007) Binding of regulatory protein Omega from *Streptococcus pyogenes* plasmid pSM19035 to direct and inverted 7-Base pair repeats of operator DNA. *J. Raman Spectrosc.*, **38**, 166–175.
20. Murayama,K., Orth,P., de la Hoz,A.B., Alonso,J.C. and Saenger,W. (2001) Crystal structure of omega transcriptional repressor encoded by *Streptococcus pyogenes* plasmid pSM19035 at 1.5 Å resolution. *J. Mol. Biol.*, **314**, 789–796.
21. Weihofen,W.A., Cicek,A., Pratto,F., Alonso,J.C. and Saenger,W. (2006) Structures of omega repressors bound to direct and inverted DNA repeats explain modulation of transcription. *Nucleic Acids Res.*, **34**, 1450–1458.
22. Otwinowski,Z. and Minor,W. (1977) Processing of X-ray Diffraction Data Collected in Oscillation Mode. *Methods Enzymol.*, **276**, 307–326.
23. Perrakis,A., Harkiolaki,M., Wilson,K.S. and Lamzin,V.S. (2001) ARP/wARP and molecular replacement. *Acta Crystallogr. D Biol. Crystallogr.*, **57**, 1445–1450.
24. Murshudov,G.N., Vagin,A.A. and Dodson,E.J. (1997) Refinement of macromolecular structures by the maximum-likelihood method. *Acta Crystallogr. D Biol. Crystallogr.*, **53**, 240–253.
25. Marston,A.L. and Errington,J. (1999) Dynamic movement of the ParA-like Soj protein of *B. subtilis* and its dual role in nucleoid organization and developmental regulation. *Mol. Cell.*, **4**, 673–682.
26. Canosa,I., Lurz,R., Rojo,F. and Alonso,J.C. (1998) β recombinase catalyzes inversion and resolution between two inversely oriented *six* sites on a supercoiled DNA substrate and only inversion on relaxed or linear substrates. *J. Biol. Chem.*, **273**, 13886–13891.
27. Carrasco,B., Ayora,S., Lurz,R. and Alonso,J.C. (2005) *Bacillus subtilis* RecU Holliday-junction resolvase modulates RecA activities. *Nucleic Acids Res.*, **33**, 3942–3952.
28. Jensen,R.B., Lurz,R. and Gerdes,K. (1998) Mechanism of DNA segregation in prokaryotes: replicon pairing by parC of plasmid R1. *Proc. Natl Acad. Sci. USA*, **95**, 8550–8555.
29. Leonard,T.A., Butler,P.J. and Lowe,J. (2005) Bacterial chromosome segregation: structure and DNA binding of the Soj dimer – a conserved biological switch. *EMBO J.*, **24**, 270–282.
30. Wang,J.D., Rokop,M.E., Barker,M.M., Hanson,N.R. and Grossman,A.D. (2004) Multicopy plasmids affect replisome positioning in *Bacillus subtilis*. *J. Bacteriol.*, **186**, 7084–7090.
31. Ebersbach,G. and Gerdes,K. (2004) Bacterial mitosis: partitioning protein ParA oscillates in spiral-shaped structures and positions plasmids at mid-cell. *Mol. Microbiol.*, **52**, 385–398.
32. Adachi,S., Hori,K. and Hiraga,S. (2006) Subcellular positioning of F plasmid mediated by dynamic localization of SopA and SopB. *J. Mol. Biol.*, **356**, 850–863.
33. Quisel,J.D., Lin,D.C. and Grossman,A.D. (1999) Control of development by altered localization of a transcription factor in *B. subtilis*. *Mol. Cell.*, **4**, 665–672.
34. Ringgaard,S., Lowe,J. and Gerdes,K. (2007) Centromere pairing by a plasmid-encoded type I ParB protein. *J. Biol. Chem.*, **282**, 28216–28225.
35. Edgar,R., Chattoraj,D.K. and Yarmolinsky,M. (2001) Pairing of P1 plasmid partition sites by ParB. *Mol. Microbiol.*, **42**, 1363–1370.
36. Hester,C.M. and Lutkenhaus,J. (2007) Soj (ParA) DNA binding is mediated by conserved arginines and is essential for plasmid segregation. *Proc. Natl Acad. Sci. USA*, **104**, 20326–20331.
37. Hu,Z., Gogol,E.P. and Lutkenhaus,J. (2002) Dynamic assembly of MinD on phospholipid vesicles regulated by ATP and MinE. *Proc. Natl Acad. Sci. USA*, **99**, 6761–6766.
38. Suefuji,K., Valluzzi,R. and RayChaudhuri,D. (2002) Dynamic assembly of MinD into filament bundles modulated by ATP, phospholipids, and MinE. *Proc. Natl Acad. Sci. USA*, **99**, 16776–16781.
39. Ebersbach,G., Ringgaard,S., Moller-Jensen,J., Wang,Q., Sherratt,D.J. and Gerdes,K. (2006) Regular cellular distribution of plasmids by oscillating and filament-forming ParA ATPase of plasmid pB171. *Mol. Microbiol.*, **61**, 1428–1442.
40. Barilla,D., Rosenberg,M.F., Nobbmann,U. and Hayes,F. (2005) Bacterial DNA segregation dynamics mediated by the polymerizing protein ParF. *EMBO J.*, **24**, 1453–1464.
41. Bouet,J.Y., Ah-Seng,Y., Benmeradi,N. and Lane,D. (2007) Polymerization of SopA partition ATPase: regulation by DNA binding and SopB. *Mol. Microbiol.*, **63**, 468–481.
42. Moller-Jensen,J., Borch,J., Dam,M., Jensen,R.B., Roepstorff,P. and Gerdes,K. (2003) Bacterial mitosis: ParM of plasmid R1 moves plasmid DNA by an actin-like insertional polymerization mechanism. *Mol. Cell.*, **12**, 1477–1487.

43. Garner,E.C., Campbell,C.S., Weibel,D.B. and Mullins,R.D. (2007) Reconstitution of DNA segregation driven by assembly of a prokaryotic actin homolog. *Science*, **315**, 1270–1274.
44. Lim,G.E., Derman,A.I. and Pogliano,J. (2005) Bacterial DNA segregation by dynamic SopA polymers. *Proc. Natl Acad. Sci. USA*, **102**, 17658–17663.
45. Hatano,T., Yamaichi,Y. and Niki,H. (2007) Oscillating focus of SopA associated with filamentous structure guides partitioning of F plasmid. *Mol. Microbiol.*, **64**, 1198–1213.
46. Barilla,D., Carmelo,E. and Hayes,F. (2007) The tail of the ParG DNA segregation protein remodels ParF polymers and enhances ATP hydrolysis via an arginine finger-like motif. *Proc. Natl Acad. Sci. USA*, **104**, 1811–1816.
47. Hiraga,S. (1992) Chromosome and plasmid partition in Escherichia coli. *Annu. Rev. Biochem.*, **61**, 283–306.
48. Laskowski,R.A., MacArthur,M.W., Moss,D.S. and Thornton,J.M. (1993) PROCHECK: a program to check the stereochemical quality of protein structures. *J. Appl. Cryst.*, **26**, 283–291.